DETECTING DISSIMILARITIES IN EM CONSTITUTIVE PARAMETERS USING DIFFERENTIAL IMAGING OPERATOR ON RECONSTRUCTED WAVE FIELD

M. I. Raza

Department of Electrical and Electronics Engineering
East West University
Dhaka-1212, Bangladesh

R. E. DuBroff

Department of Electrical and Computer Engineering
Missouri University of Science and Technology
Rolla, MO 65409, USA

Abstract—Electromagnetic field will scatter when incident on boundaries separating media with different constitutive parameters. This paper demonstrates the use of a differential operator on recorded scattered waves to reveal the shape of the boundary. The method is noninvasive and is composed of three phases. First, the area of interest is illuminated and the resulting scattered electromagnetic fields are recorded. In the 2nd phase, the captured data is numerically reverse simulated in time to reconstruct the field distribution in the region of interest. Finally, the differential imaging operator is applied on the reconstructed wave field, creating an image delineating the boundary where scattered fields originated. This technique does not require the knowledge of location of the boundaries nor the nature of the discontinuity in the constitutive parameters. The proposed imaging system is scalable, whereby modification of the source signal, recorder sampling, and numerical model allows imaging objects of smaller dimensions and creation of sharper and more accurate images.

1. INTRODUCTION

Non-invasive techniques for object detection and characterization are widely used in different fields, ranging from medical imaging to oil and gas exploration [1–4]. There are some established methods

---

Corresponding author: M. I. Raza (iraza@ewubd.edu).

such as reverse migration and inverse extrapolation techniques which have been used widely [5–8]. Recent advances demonstrate different methods used in imaging such as Electrical Capacitance Tomography (ECT) and Radio Frequency Tomography [9–13]. In most of these approaches different numerical techniques are used to process data. Most of these techniques work either in frequency domain or rely on transmitted waves for image construction. The cost and constraints of computing has till recently limited the use of time domain methods. However, with increased computing power and speed at ever decreasing cost has diverted research focus to the finite-difference time-domain (FDTD) method. It is now a research friendly tool and has evolved to be one of the more preferred numerical methods [14].

An approach using the FDTD method was earlier demonstrated for detecting objects in acoustic media using radiation imaging operators (RIO) [15, 16]. In this paper the non-invasive RIO method is used to detect boundaries of unknown objects embedded in known electromagnetic medium. The boundary is the interface that separates the object and the surrounding media. The object is assumed to have constitutive parameters different from the surrounding media. These parameters, such as permittivity, permeability, and loss tangent, define the material characteristic impedance, field propagation velocity, and electromagnetic wave field distribution. These RIOs for boundary imaging is derived from Maxwell's electromagnetic wave equation. Application of the RIO operator in this paper is limited to detecting boundary in several usages model demonstration. For simplification, the difference in the object and surrounding media material properties is limited to dielectric constant (relative permittivity). The permeability is assumed constant and the material is considered lossless across the region of interest.

Physical setup of typical imaging problems can generally be defined by schematic shown in Fig. 1. The object is assumed to be embedded in a region of known physical characteristics. It is assumed that the primary reflection originates from the object boundary delineating the first change in material characteristics. The source excitation is placed in an accessible area located somewhere not too far from the object. If the distance is significant, the energy in the scattered waves may not be sustainable above the noise floor. A set of recorders is placed closed to the source in the least intrusive method. The location of the source and the object to be imaged has to be on opposite sides of the recorders. It is assumed that the first reflection is significant compared to the secondary reflections and thus the latter is neglected. The technology is scalable as it allows better imaging resolution by using source signal with higher harmonic content. To
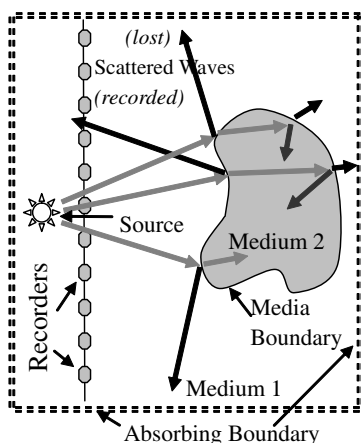
Figure 1. 2D problem space for non-invasive boundary detection.

improve the resolution of the imaged boundary increased recorder density must also be deployed near the source.

2. IMAGING OPERATOR FOR ELECTROMAGNETIC INTERFACE

Wave propagation is defined by Maxwell's equation, a 2nd order partial differential equation (PDE). For electric field in 3D Cartesian space, i.e., rectangular coordinates, the equation is given by

$$\left(\frac{\partial^2}{\partial x^2} + \frac{\partial^2}{\partial y^2} + \frac{\partial^2}{\partial z^2} - \mu\varepsilon\frac{\partial^2}{\partial t^2} \right) \bar{E} = 0 \tag{1}$$

A simplified two dimensional TM mode wave propagation case is studied in this paper. It is assumed that field distribution is constant in the z direction, i.e., $\partial z = 0$. The 2D electromagnetic (EM) fields are defined by the following vectors,

$$\bar{E} = E_z\hat{z} \quad \text{and} \quad \bar{H} = H_x\hat{x} + H_y\hat{y}$$

As shown above, the electric field has only z components (as indicated by the unit vector $\hat{z}$), while the magnetic field has both x and y components (as indicated by unit vectors $\hat{x}$ and $\hat{y}$). Using D to represent the partial differential operator, wave Equation (1) for the electric field simplifies to,

$$\left(D_{xx}^2 + D_{yy}^2 - \frac{1}{c^2}D_{tt}^2 \right) E_z = 0, \text{ (with velocity, } c = 1/\sqrt{\mu\varepsilon}).$$

The PDE operator is factored to support wave propagation primarily in the $\pm y$ direction. Hence, the corresponding wave equation satisfying fields in medium 2 (object) with assumed velocity $c_2 = 1/\sqrt{\mu_2 \varepsilon_2}$ is

$$\left(D_{yy}^2 - \frac{1}{c_2^2} \left(D_{tt}^2 - c_2^2 D_{xx}^2 \right) \right) E_{2z} = 0$$

$$\left(D_{yy}^2 - \left(\frac{1}{c_2} D_t \sqrt{1 - c_2^2 \frac{D_{xx}^2}{D_{tt}^2}} \right)^2 \right) E_{2z} = 0$$

The square root term in the differential operator is expanded using Taylor series. In the problem space being considered, the object is located in the $+y$ direction with reference to the source. On the surfaces of the object close to the source, the phase velocity y component of EM field will be stronger than the phase velocity x component as the wave front will be propagating primarily in the y direction. Hence, the ratio of the 2nd order derivative of the EM field in x direction to the 2nd order time derivative of the EM field will be small. Thus, the terms in the expansion that are 2nd order and above is neglected. So,

$$\left(c_2 D_{yt}^2 + D_{tt}^2 - \frac{1}{2} c_2^2 D_{xx}^2 \right) E_{2z} = 0$$

The reduced RIO operator consists of three 2nd order partial derivatives of the electric field propagating in the remote object, i.e., medium 2. Using appropriate boundary conditions (b.c.) valid on the boundary of the two media, the differential operator is then transformed to be a function of the electric field on the medium 1 side of the boundary.

The EM field b.c. define that the electric flux density component (D) normal to the boundary in a charge free region is the same on both sides of the boundary, i.e., $D_{n1} = D_{n2}$. Similarly, the tangential electric field components (E) are the same on both sides of the boundary, i.e., $E_{t1} = E_{t2}$. These conditions are necessary to derive the imaging operator for electromagnetic media. For this particular setup, the electric field component E_z in both the regions is tangential to the boundary of the object, irrespective of the object surface orientation in the x-y plane. Therefore,

$$E_{1z}|_{boundary} = E_{2z}|_{boundary} \tag{2}$$

$$\text{or } \bar{E}_1 = E_{z1} e^{j\omega t} \hat{z} = E_{z2} e^{j\omega t} \hat{z} = \bar{E}_2$$

Therefore, EM field z-component on both sides of the boundary will be continuous on the boundary in both space and time, meaning

that the fields are differentiable both spatially in the x-y direction and in the time domain.

$$\frac{\partial^2 \left(E_{z1}e^{j\omega t}\right)}{\partial t^2} = \frac{\partial^2 \left(E_{z2}e^{j\omega t}\right)}{\partial t^2}$$

$$\frac{\partial^2 \left(E_{z1}e^{j\omega t}\right)}{\partial x^2} = \frac{\partial^2 \left(E_{z2}e^{j\omega t}\right)}{\partial x^2}$$

$$\frac{\partial^2 \left(E_{z1}e^{j\omega t}\right)}{\partial yt} = \frac{\partial^2 \left(E_{z2}e^{j\omega t}\right)}{\partial yt}$$

Therefore the RIO for $+ve$ y going waves on the media 1 side of the boundary can be rewritten as below,

$$\left(c_2 D_{yt}^2 + D_{tt}^2 - \frac{1}{2}c_2^2 D_{xx}^2\right) E_{1z} = 0 \tag{3}$$

It must be noted that Equation (3) will only be satisfied at the boundary of the object. The above RIO will be applied to the reconstructed E_z field. The data is reconstructed through simulation and data acquisition methods. As will be discussed later, due to data gathering in remote detection scheme, field distribution can only be true in region 1, particularly in the area between the recorders and the object. It will however be invalid in region 2 as wave reconstruction through reverse simulation in the object cannot be accomplished as the object physical characteristics, location, and boundary is not known. As the tangential boundary conditions in Equation (2) are valid only at the boundary, Equation (3) will return a minimum value only at the boundary. This premise will be used to reconstruct the object boundary.

3. ALGORITHM FOR IMAGE RECONSTRUCTION

The algorithm for creating an image has both a data collection phase and a computational phase. The data collection phase has to be properly designed to maximize signal to noise ratio. This basically entails using recorders that have good noise rejection capability and high level of recorder sensitivity. The recorder sensitivity is vital as the scattering from the object interface will be soft compared to the source signal level. The recorded signal will be analog in nature. The analog data will have to be sampled for computational analysis. The quantization level of the analog to digital converter (ADC) must be small to be able to accurately characterize the received signals and also improve resolution of the final image.

The first step of the proposed process is field data collection. In this step the source is initially excited in the region of concern while recorders are placed strategically to acquire, i.e., measure data scattered by the sought object. In a practical setup the source will be an electromagnetic pulse generating device. The source used in this experiment is defined by a pulse which consists of a limited frequency range of interest. As the bandwidth of the pulse increases, the wavelength of the harmonic content of the signal reduces. Smaller wavelength will allow higher resolution of the object boundary to be imaged. As a rule of thumb, the smallest feature of the object boundary must be no less than 20 times the wavelength of the significant harmonic in the pulse. This concept is widely used in high frequency analysis in signal integrity and antenna engineering where a physical dimension is considered to be lumped when it is smaller than $\lambda/20$, where λ is the wavelength [17]. This data acquisition phase is implemented for this concept paper using numerical simulations. It should be noted that the field distribution that were not or could not be recorded are lost and will not be available for image reconstruction.

When the source excitation is engaged, it is assumed there is no significant electromagnetic energy distribution in the region (quiet). The energy that exists has to be below an acceptable noise floor. When the source is excited, a string of recorders are turned on to record the analog electromagnetic field. In this analysis the recorders are assumed to be placed at uniform intervals, though it is not a necessary condition. The nature of the recorder placement has more to do with how best the scattered waves can be reconstructed. An initial screening can be conducted as a first step with uniform recorder placement with the intent to identify where the most changes in the recorded scattered fields are observed. Based on that data receiver locations can be modified to increase density in a region where the variations of scattered data is most. Recent work is ongoing where recorder and sensor placement sensitivity is being studied [18]. The recorders only capture select electric field components which are necessary for this imaging exercise. The data is recorded for sufficient length of time until the primary reflected field from the image has been recorded. Name this data S_{field}. The secondary reflections are not required as the boundary conditions are satisfied with the first scattered wave reconstruction. Also, secondary reflections are typically due to scattering from other layers. The length of recorded data has to be sufficient such that the overall distribution of electric field in the region of interest has become quiet or static. This is necessary to allow for initialization of the region of interest during simulation. It is assumed that the field distribution is near zero (or static).

In the next step (step 2), the region of interest is modeled without the sought object. The numerical space is modeled as a homogeneous region, with known characteristics. It should be noted that the object (being imaged) shape, location, or characteristics is not known at this stage. A source, similar to the one used in step 1, is modeled as source excitation. As the simulation progresses in discretized time, the wave distribution across the whole simulated space is stored at every time step. The finer the grid, the more accurate is the simulated wave propagation. However, physical and cost constraints limit the number and frequency of recorders used in the field (step 1). The recorders used in the 2nd step are also modeled similarly. Data is recorded at the locations where the actual recorders were placed in step 1. Call this S_{src}. The data at all the nodes in the simulation space is also recorded, D_{src}. This data is needed for the reconstruction of the wave field distribution.

Next, reverse wave propagation is simulated using the numerical simulation algorithm. In this part of step 2, the source in steps 1 or 2 is not used as excitation. Rather, only the scattering waves that were recorded in step 1 is used as source signal. The scattering data S_{scat}, which originated from the boundary of the object in step 1 is calculated by subtracting incident pulse propagation recorded in step 2, i.e., S_{src}, from the data captured in the recorders in the field S_{field}, which includes both the incident and the scattered wave field, hence,

$$S_{scat} = S_{field} - S_{src}$$

In this simulation phase, wave propagation is backward simulated in time using the same numerical simulation setup, again assuming homogeneous model space excluding the object from model space. It should be noted that the object location, shape, size is not yet known. During backward simulation of the scattered waves, the wave fields at every node in the region of interest are also recorded. Call this data D_{scat}. The reverse simulation recreates the scattered wave distribution in the time domain, at every time-step. The sum of D_{scat} and D_{src} will reconstruct the wave distribution D_{recon} in the area between the recorders and the object boundary.

$$D_{recon} = D_{scat} + D_{src}$$

This reconstruction will only be valid in the space between the recorders and the boundary. There are scattered data that propagates in directions where no recorders are present. As these scattered waves from the boundary cannot be captured by recorders, this data cannot be made available during wave reconstruction. Particularly regions that are located near the boundary of the model space cannot be reconstructed due to the absence of recorded scattered waves. As a

result, these object boundaries are lost in the reconstructed image — more aptly called 'dead zones'. The size of the dead zone is larger when the recorder is farther away from the object. It is therefore advisable to have a wide string of recorders close to the unknown object. Ray theories are very good in determining what waves will be captured by the recorders and what will be lost in the absorbing or radiation boundaries.

An apparent reconstruction of the waves beyond the boundary also takes place automatically. However, the reconstructed wave will not be valid in the object area and thus wave reconstruction in regions away from the object boundary will not be real. Therefore, the result of the operation of the PDE on this data will be meaningless and be erroneous.

The final step is the extraction of the image. At this stage the RIO is applied to the reconstructed data and processed (normalized). The result of this data operation will show a minimum only at the boundary of the object. As the result of the operator across the space is plotted, a low will show only where the boundary of the object facing the source is located. The reason this part of the object edge is detected is because scattering from only this segment of boundary is reliably measured by the recorders.

4. IMAGE SPACE SIMULATION AND ANALYSIS

The reconstruction of the scattered wave is implemented using the finite difference time domain (FDTD) numerical method [19]. FDTD is used to generate all the numerical data for both forward and backward wave propagation. Fields at the numerical nodes are all initialized to zero, assuming that the field distribution is below the noise floor. The scattered data stored at the recorder locations are played backwards in time as the simulation is run in reverse. The simulation starts at the last recorded time step and decrements to zero. The greater the density of the recorders used in the field data acquisition state, the better the information available for back propagation during scattered wave reconstruction. The smaller the wavelength of the harmonics of the pulse, the lesser the distance needed between the recorders (less than $\lambda/20$). Absence of data between recorder nodes can be partially compensated using numerical interpolation techniques [20].

The Maxwell's equations that are modeled to simulate wave propagation in two dimensions (2D) are given by

$$\varepsilon_0 \frac{\partial E_{zx}}{\partial t} + \sigma_{ex} E_{zx} = \frac{\partial H_y}{\partial x} \quad \text{and} \quad \varepsilon_0 \frac{\partial E_{zy}}{\partial t} + \sigma_{ey} E_{zy} = -\frac{\partial H_x}{\partial y}$$

$$\mu_0 \frac{\partial H_x}{\partial t} + \sigma_{my} H_x = -\frac{\partial (E_{zx} + E_{zy})}{\partial y}$$

$$\text{and } \mu_0 \frac{\partial H_y}{\partial t} + \sigma_{mx} H_y = \frac{\partial (E_{zx} + E_{zy})}{\partial x}$$

Discretizing the RIO using 2nd order finite difference,

$$\partial_{yt}^2 Ez_{i,j}^{n+1} = \frac{Ez_{i,j+1}^{n+2} - Ez_{i,j+1}^{n} - Ez_{i,j-1}^{n+2} + Ez_{i,j-1}^{n}}{4\delta_t \delta_y} \tag{4}$$

$$\partial_{tt}^2 Ez_{i,j}^{n+1} = \frac{Ez_{i,j}^{n+2} - 2Ez_{i,j}^{n+1} + Ez_{i,j}^{n}}{\delta_t^2} \tag{5}$$

$$\partial_{xx}^2 Ez_{i,j}^{n+1} = \frac{Ez_{i+1,j}^{n+1} - 2Ez_{i,j}^{n+1} + Ez_{i-1,j}^{n+1}}{\delta_x^2} \tag{6}$$

The discretized radiation imaging operator is then given by

$$RIO_{i,j} = \frac{c_0}{\sqrt{\varepsilon_r}} \partial_{yt}^2 Ez_{i,j}^{n+1} - \partial_{tt}^2 Ez_{i,j}^{n+1} + \frac{c_0^2}{2\varepsilon_r} \partial_{xx}^2 Ez_{i,j}^{n+1} \tag{7}$$

A hard voltage source is used to generate a Gaussian pulse, given by $s(t) = Ke^{-\left(\frac{t-A}{B}\right)^2}$.

The description of the simulation model is shown in Fig. 2. The numerical values of the model parameters are also given.

The pulse width parameters (A and B) in time-steps are set to $20dt$, necessary to define the bandwidth of the Gaussian pulse excitation. Berenger's perfect latched layer (PML) attenuating layers are used in this numerical method [21]. The rapid attenuation of the
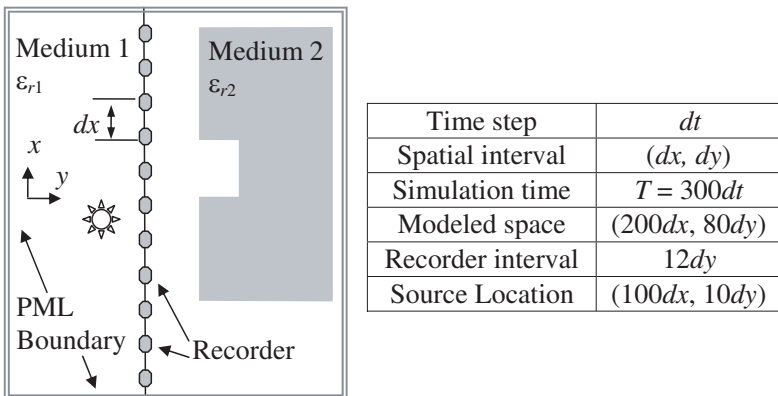

Time step	dt
Spatial interval	(dx, dy)
Simulation time	$T = 300dt$
Modeled space	$(200dx, 80dy)$
Recorder interval	$12dy$
Source Location	$(100dx, 10dy)$

Figure 2. Simulation space for imaging operator.

waves incident in these layers near the boundary of the numerical space, results in very negligible reflection from the edge of numerical space model, thereby simulating wave propagation into infinite space. Depth of PML layer used in this simulation was 6.

5. SIMULATION RESULTS AND DISCUSSION

Matlab scripts are used to simulate wave propagation and implement the RIO [22]. Different object shapes are used to evaluate the algorithm and the proposed methodology. In the first set of analysis, the width of the Gaussian pulse is varied to show the effect of varying pulse width on the quality of the image. The exercise compared images generated with a width of 10, 20, 30, and 40 time intervals for the pulse. A narrow pulse will have higher harmonics. However, the narrow pulse generates an aliasing effect on the image it produces. A wide pulse on the other hand has lesser harmonics and thus produces an image which is less sharp. The blurriness of the image reduces the accuracy of the boundary detected (see Fig. 3).

Another set of experiments were run to demonstrate the ability of the method to detect a recess. It could either be a hole or simply a recess. Data shows that the hole is detected well when it has dimensions no less than $10dx$, where dx is the space interval (see Fig. 4). When object boundary features of sizes smaller than $10dx$ is to be
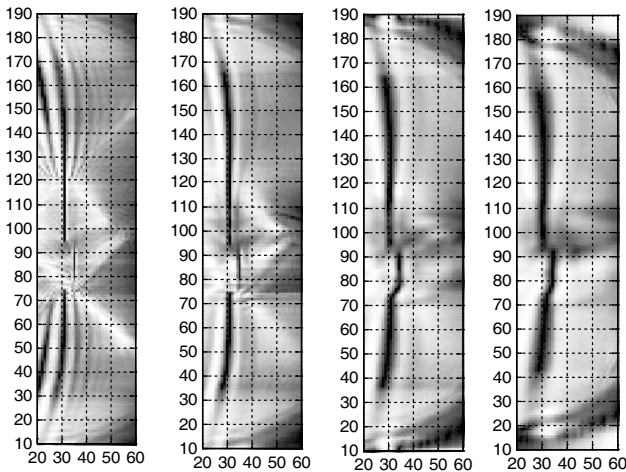
Figure 3. Effect of source pulse width on boundary image (pulse width parameter, from left, $B = 10, 20, 30, 40dt$).

detected, the source signal must be modified to have a signal source with harmonic content designed to meet the imaging requirements. A plot of the incident Gaussian pulse in the prescribed configuration along with the scattered pulse is shown in Fig. 5. The plot shows all three non-zero EM components.
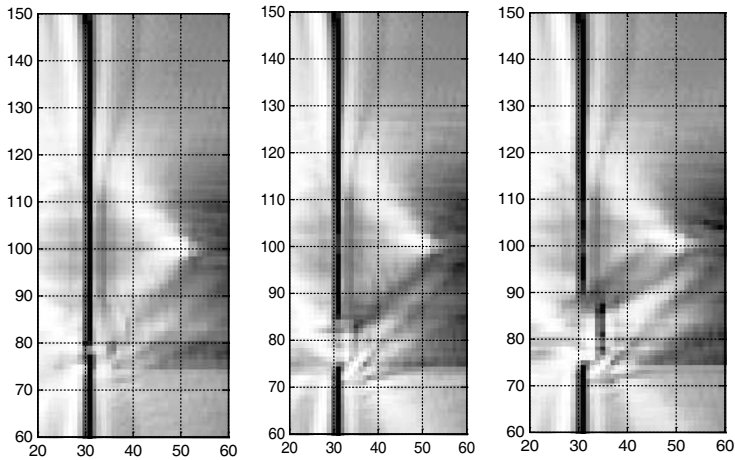
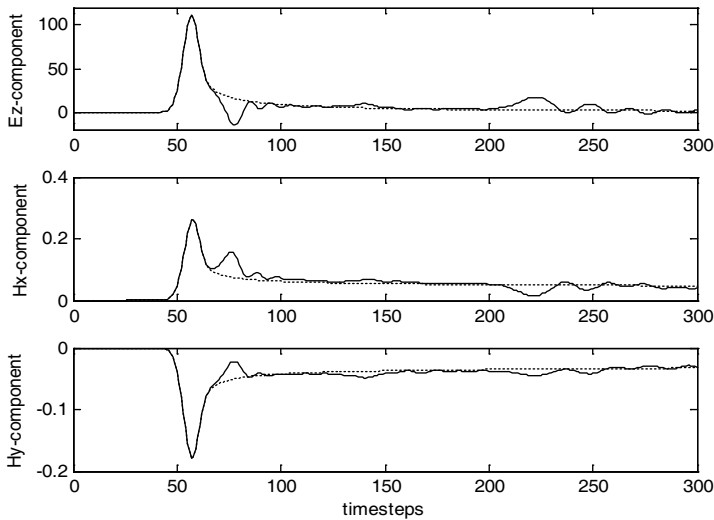**Figure 4.** Detection of recess (from left, width of recess = 75–80, 75–85, 75–95), while $B = 20$.

Figure 5. Incident wave (dashed line) and scattered wave (solid line) as captured by recorders.
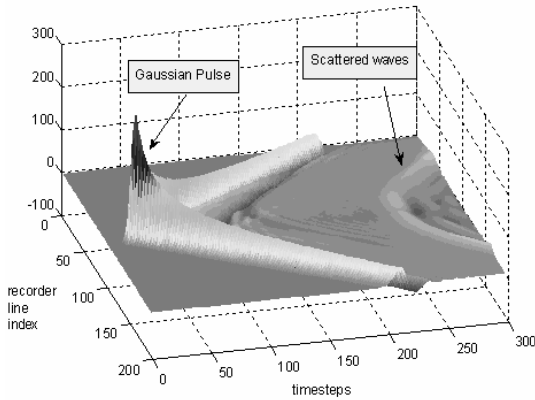
Figure 6. A 3D view of the wave propagation as recorded on the recorder string.
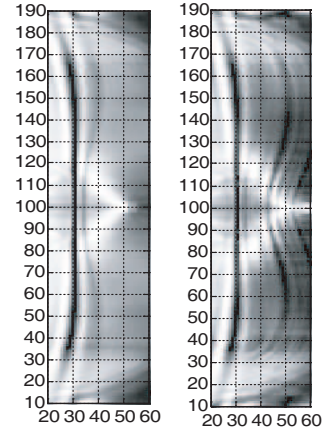
Figure 7. Imaging of objects of different thickness.

A 3D plot of the propagating E_Z is also shown in Fig. 6. The wave plot shows the field as recorded on the recorder string. As observed in the simulation results, the initial wave front is the incident wave field which propagates from the source towards all directions including the object. Right behind the incident pulse is the scattered wave front, as reflected from the object interface.

The proposed procedure uses scattered data to construct an image of the boundary. The primary scattering from the object is defined by the difference in the material characteristics of the two medium. Hence the initial scattered wave front is not a function of how thick the object is (Fig. 7). However, the secondary reflection from the second interface can have either a constructive or destructive effect on the primary scattering (Fig. 8). Nevertheless the secondary wave front will be time-delayed; hence correction method can be developed to fix this interference.

The application of the RIO concept in this paper has been limited to two dimensions (2D). Work is on going on the extension of this concept to three dimensions (3D). A 3D operator will be based on the same boundary condition requirements, i.e., continuity of tangential components and select derivatives at the object surface. The wave fields in the region will have to be reconstructed using 3D backward simulation. The operator will then create a 3D image showing a low at the locations where the boundary of the objects faces the sources. It should however be noted that the extent of simulation computation
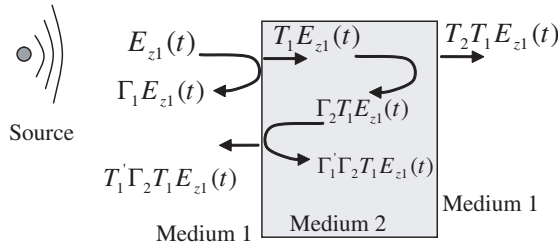
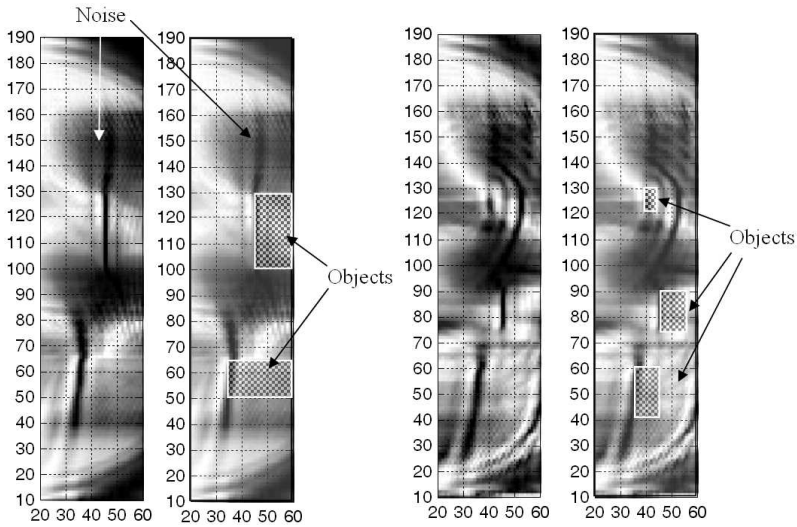**Figure 8.** Multiple scattering wave fronts due to multilayer object.

Figure 9. Images of source facing boundary of multiple object examples. The objects all have relative permittivity of 3.5, while embedded in air type media.

necessary for the 3D problem will be significantly higher than a 2D problem. This is due to leap frog increase in the field nodes in spatial dimensions due to the additional space variable. However, given the increased computing power of current simulation engines, computation time and resource is not a significant problem.

6. CONCLUSION

This paper has successfully demonstrated the use of differential operators to detect object boundaries in electromagnetic domain. The

operator has used the recorded reflected waves to reconstruct wave distribution. This method identifies the side of the boundary that faces the source. The problem discussed here has been limited to TM mode and 2D configuration. However, simple expansion of the simulation and experimental setup can provide for a more diverse setup. The scalability of this method to detect small features can be accommodated with shorter source pulses and faster sampling rates. The simplicity of the data collection mechanism and the easy simulation based scattered wave reconstruction makes the methodology easy and quick.

Given its non-intrusive nature, the application scope of this method is wide, particularly in the area of medical engineering. In this field it is often necessary to detect and accurately locate abnormal growth such as tumors, which are features embedded in relatively uniform tissue [23]. The proposed methodology can be used to locate similar growth. Results presented in Fig. 9 show how multiple embedded features with varying characteristic parameters are detected.

REFERENCES

1. Blackledge, J. M. and L. Zapalowski, "Quantitative solutions to the inverse scattering problem with applications to medical imaging," *Inverse Problems*, Vol. 1, 17–32, 1985.

2. Zhou, H., T. Takenaka, J. E. Johnson, and T. Tanaka, "A breast imaging model using microwaves and a time domain three dimensional reconstruction method," *Progress In Electromagnetics Research*, PIER 93, 57–70, 2009.

3. Kuster, M., et al., "Acoustic imaging in enclosed spaces: Analysis of room geometry modifications on the impulse response," *J. Acoust. Soc. Am.*, Vol. 116, No. 4, Pt. 1, 2126–2136, Oct. 2004.

4. Niendorf, T. and D. K. Sodickson, "Highly accelerated cardiovascular magnetic resonance imaging: Concepts and clinical applications," *Proceedings of the 28th IEEE EMBS Annual International Conference*, 373–376, New York City, USA, Aug. 2006.

5. Wapenaar, C. P. A., G. L. Peels, V. Budejick, and A. J. Berkhout, "Inverse extrapolation of primary seismic waves," *Geophysics*, Vol. 54, No. 7, 853–863, Jul. 1989.

6. Goharian, M., M. Soleimani, and G. Moran, "A trust region subproblem for 3D electrical impedance tomography inverse problem using experimental data," *Progress In Electromagnetics Research*, PIER 94, 19–32, 2009.

7. Chang, W. F. and G. A. Cahon, "3D acoustic reverse-time migration," *Geophysical Prospecting,* Vol. 37, 243–256, Apr. 1989.

8. Stolt, R. H., "Migration by fourier transform," *Geophysics*, Vol. 43, 23–48, Feb. 1978.

9. Lei, J., S. Liu, Z. H. Li, and M. Sun, "Image reconstruction algorithm based on the extended regularized total least squares method for electrical capacitance tomography," *IET Science, Measurement & Technology*, Vol. 2, 326–336, Sep. 2008.

10. Yu, J., Z. Huang, H. Ji, B. Wang, and H. Li, "Image reconstruction algorithm of electrical resistance tomography for the measurement of two-phase flow," *Proceedings of IEEE Sensors*, Vol. 1, 63–66, Oct. 2003.

11. Lam, K., M. J. Yedlin, and C. G. Farquharson, "Two-dimensional radio frequency tomography," *IEEE Trans. Microw. Theory Tech.*, Vol. 55, No. 4, 801–808, Apr. 2007.

12. Soleimani, M., C. N. Mitchell, R. Banasiak, R. Wajman, and A. Adler, "Four-dimensional electrical capacitance tomography imaging using experimental data," *Progress In Electromagnetics Research,* PIER 90, 171–186. 2009.

13. Soleimani, M., "Simultaneous reconstruction of permeability and conductivity in magnetic induction tomography," *Journal of Electromagnetic Waves and Applications*, Vol. 23, No. 5–6, 785–798, 2009.

14. Winton, S. C., P. Kosmas, and C. M. Rappaport,, "FDTD simulation of TE and TM plane waves at nonzero incidence in arbitrary layered media," *IEEE Trans. Antennas Propagat.*, Vol. 53, No. 5, 1721–1728, May 2005.

15. DuBroff, R. I., M. I. Raza, and T. J. Herrick, "Remote detection of acoustic boundaries using radiation imaging operators," *IEEE Trans. Ultrason., Ferroelect., Freq. Contr.*, Vol. 42, 1012–1019, Nov. 1995.

16. Raza, M. I., R. I. DuBroff, and J. L. Drewniak, "Radiation imaging operators applied to the detection of velocity and density contrast boundaries," *IEEE Trans. Ultrason., Ferroelect., Freq. Contr.*, Vol. 44, 1401–1404, Nov. 1997.

17. Pozar, D. M., *Microwave Engineering*, 2nd Edition, John Wiley & Sons, 2004.

18. Pan, P. and D. Schonfeld, "Image reconstruction and multidimensional field estimation from randomly scattered sensors," *IEEE Trans. Image Processing*, Vol. 17, 94–99, Jan. 2008.

19. Taflove, A. and S. C. Hagness, *Computational Electrodynamics:*

The Finite-difference Time-domain Method, 3rd edition, Artech House, Boston, MA, Jun. 30, 2005.

20. Hira, A., S. A. Hossain, and M. I. Raza, "Interpolation techniques to improve RIO boundary detection," *PIERS Proceedings*, 1234–1238, March 23–27, Beijing, China, 2009.

21. Berenger, J. P., "Perfect matched layer for the FDTD solution of wave-structure interaction problems," *IEEE Trans. Antennas Propagat.*, Vol. 44, 110–117, Jan. 1996.

22. www.mathworks.com, MATLAB$^{\textcircled{R}}$, Version 7, Release 14.

23. Zhang, H., S. Y. Tan, and H. S. Tan, "A flanged parallel-plate waveguide probe for microwave imaging of tumors," *Progress In Electromagnetics Research*, PIER 97, 45–60, 2009.